Water Air Soil Pollut (2025) 236:56
https://doi.org/10.1007/s11270-024-07630-3

Synthesis and Characterization of Efficient Adsorbents for Methylene Blue Based on Graphene Oxide/β-cyclodextrin Composites

Yanping Qu · Hongcui Li · Ibrahim Yakub · Wen He · Wenchan Dong · Mohamad Hardyman Barawi · Sirui Wang · Huimin Ma · Zhenpeng Zhu

Received: 12 June 2024 / Accepted: 6 November 2024

Abstract In this paper, a novel graphene oxide/β-cyclodextrin composite (GO/β-CD) adsorbent was synthesized for the effective simultaneous removal of dyes. GO and GO/β-CD were characterized using BET, SEM, FT-IR, Raman, and XRD techniques. GO/β-CD has a BET specific surface area of 0.25 m^2/g. The surface of GO/β-CD contains a significant number of reactive groups, such as carboxyl groups, which enable the effective adsorption of methylene blue (MB). The adsorption of GO/β-CD on methylene blue (MB) in aqueous solution was also investigated kinetically and thermodynamically. The kinetic and thermodynamic parameters of the reaction were calculated. Based on the experimental results, the adsorption reaction was determined to be a spontaneous endothermic reaction. The adsorption of MB on GO/β-CD best fit the Langmuir model based on the results of the adsorption isotherm model fitting. The maximum adsorption capacity of the composite was 434.78 mg/g. The GO/β-CD adsorbent was highly efficient at adsorbing cationic dyes, and its performance remained consistently high after six cycles. Thus, GO/β-CD offers the advantages of nontoxicity, excellent adsorption and regeneration properties, and great potential for treating real and simulated wastewater from various industries.

Keywords Absorbent · β-cyclodextrin · Graphene oxide · Methylene blue

Y. Qu (✉) · H. Li · W. He · S. Wang · H. Ma · Z. Zhu
College of Biological and Chemical Engineering, Qilu Institute of Technology, Jingshi Dong Road 3028, Zhangqiu District, Jinan 250200, China
e-mail: 805025846@qq.com

I. Yakub
Department of Chemical Engineering and Energy Sustainability, Faculty of Engineering, Universiti Malaysia Sarawak, Jalan Dato Mohd Musa, 94300 Kota Samarahan, Sarawak, Malaysia

W. Dong
State Key Laboratory of Biobased Material and Green Papermaking, Key Laboratory of Pulp & Paper Science and Technology of Shandong Province/Ministry of Education, Qilu University of Technology, Shandong Academy of Sciences, Jinan 250353, China

M. H. Barawi
Faculty of Cognitive Sciences and Human Development, Universiti Malaysia Sarawak, Jalan Dato Mohd Musa, 94300 Kota Samarahan, Sarawak, Malaysia

1 Introduction

With the acceleration of economic development and urbanization, sewage discharge from industries such as printing and dyeing is seriously polluting the environment. Azo dyes present in wastewater from the textile, dyeing, and leather industries are being released into natural water bodies. This leads to environmental degradation and serious health damage through the food chain. Through investigations, more than 10,000 dyes are being produced worldwide,

Published online: 19 December 2024

generating 700,000 tons of dye wastewater (Samsami et al., 2020). Among them, methylene blue (MB) is widely used for dyeing products such as cotton, paper, and wool. Due to its high chromaticity, even at low concentrations in water, it can impede plant photosynthesis, reduce the oxygen content of water bodies, and inhibit the reproduction and growth of aquatic plants and animals. Due to its aromatic ring structure and the presence of nitrogen and sulfur, methylene blue is carcinogenic and nonbiodegradable (Din et al., 2021; Raees et al., 2021), which can lead to bioconcentration. Prolonged contact with human skin can result in structural and functional changes in human cells, potentially causing lesions and cancers (Yu et al., 2021). Ingestion can lead to an increased heart rate, vomiting, nausea, jaundice, tissue necrosis, and limb paralysis and has a significant impact on the ecosystem (Rápó & Tonk, 2021).

Currently, treatment methods for this class of dye wastewater include coagulation, adsorption, advanced oxidation, membrane, and biological methods (Rápó & Tonk, 2021). However, most of these methods have limitations, such as generating toxic sludge and incurring high operation and maintenance costs. Among these methods, adsorption has been widely recognized as a cost-effective technique for treating dye wastewater (Abd El Salam, 2023; Koçak et al., 2024; Sadiq et al., 2021). The commonly used adsorbents include activated carbon, natural clay, anionic resin, and silica gel. Nevertheless, these adsorbents have certain limitations, such as a slow absorption rate, small adsorption capacity, and high energy consumption during regeneration (Nguyen et al., 2021; Osagie et al., 2021). Consequently, the advancement of efficient adsorbents is crucial not only for improving the removal efficiency of dye-containing wastewater and reducing both treatment duration and costs but also for attaining effective, cost-efficient, and sustainable water pollution management.

In recent years, cyclodextrin polymers have been applied for environmental remediation. β-Cyclodextrin (β-CD) is a cyclic macromolecule with a unique conical cavity containing seven α-(1,4)-linked glycosyl units (Ching et al., 2022). The carbon−hydrogen bonds in the cyclodextrin molecule are connected by acetal-oxygen ether rings. The cavity exhibits hydrophobic properties due to the carbon−hydrogen bonding force, allowing it to accommodate small molecules of various particle sizes. The outer cavity of β-CD is hydrophilic. Its unique cone-shaped structure comprises 7 C_6 position primary hydroxyl groups in the upper part and 14 C_2 and C_3 position secondary hydroxyl groups in the lower part. The hydroxyl functional group is relatively active, making it hydrophobic and suitable as an active site for chemical modification (Xu et al., 2022). At the same time, cyclodextrins are low-cost, nontoxic, and biodegradable.

However, cyclodextrins are difficult to apply directly because of their high solubility in water. Cyclodextrins and their derivatives are frequently polymerized with cross-linking agents containing bifunctional or multifunctional groups to produce cyclodextrin-cross-linking polymers (Li et al., 2022; Ozelcaglayan & Parker, 2023). Nonetheless, polymerization solely with cross-linking agents reduces the adsorption capacity of cyclodextrin polymers. On the other hand, cyclodextrin polymers obtained by using epichlorohydrin as a cross-linking agent have a relatively high cyclodextrin mole fraction and form a three-dimensional reticular spatial structure. Still, their mechanical strength is not optimal, which limits their application. Additionally, flexible cross-linkers, such as citric acid, are easily entangled due to the flexibility of their molecular chains. This results in the nonporous structure of cyclodextrin polymers, which have a small specific surface area and slow mass transfer rate, making it difficult to achieve the desired adsorption effect (H. Demircan Ozelcaglayan et al., 2024; Liu et al., 2011). Although cyclodextrin polymers are inexpensive and highly regenerative, most cyclodextrin polymers currently in use are nonporous and have a specific surface area of less than 10 $m^2 \cdot g^{-1}$ (Crini & Morcellet, 2002; Jemli et al., 2024). It has been shown that introducing carriers into polymers facilitates the formation of pores, increasing the specific surface area and improving the adsorption capacity. For example, Muhammad Usman (Usman et al., 2021) synthesized a new adsorbent, nitrilotriacetic acid β-cyclodextrin chitosan (NTA-β-CD-CS), using chitosan as a carrier with a high specific surface area. This adsorbent was used for the effective simultaneous removal of dyes and heavy metals. The maximum adsorption capacities for Hg(II), MB, and methyl orange (MO) were 178.3, 162.6, and 132.5 mg/g, respectively.

Graphene oxide (GO) is a novel two-dimensional carbon nanomaterial with a high specific surface

area and abundant oxygen-containing groups (e.g., carboxyl, hydroxyl, epoxy) (Bahadi et al., 2024; Chowdhury et al., 2013). The introduction of oxygen-containing functional groups has endowed graphene oxide with rich chemical properties, making it easy to synthesize composites with various functions as a carrier. Moreover, the GO surface is negatively charged and has a high adsorption capacity for cationic dyes such as methylene blue. The adsorption mechanism mainly includes hydrogen bonding, electrostatic interactions, and π-π interactions (Shi et al., 2022; Yilmaz, 2022); therefore, in the present study, we used GO as a carrier with β-CD for the synthesis of graphene oxide/β-cyclodextrin composites (GO/B-CD). The inclusion of GO aims to overcome the technical problem of spatial collapse due to the intertwining of polymer molecular chains. This results in the formation of an adsorbent with a high specific surface area, microporous structure, and ultrahigh adsorption capacity for cationic dyes (Z. Yang et al., 2021; L. Fu et al., 2015). The structural and functional characteristics of the efficient adsorbent GO/β-CD were systematically investigated using scanning electron microscopy (SEM), Fourier-transform infrared spectroscopy (FT-IR), Brunauer–Emmett–Teller (BET) analysis, Raman spectroscopy, and X-ray diffraction (XRD). A comprehensive elucidation of the adsorption mechanisms was achieved by integrating insights from adsorption kinetics, thermodynamics, and isotherm models. This study is intended to offer theoretical underpinning for the application of cyclodextrin polymers and the effective removal of dyes from aqueous systems.

2 Experiments

2.1 Experimental Reagents

β-Cyclodextrin (β-CD > 99.9%) was purchased from Adamas Reagent Ltd., China. Graphene oxide (GO) was purchased from Shenzhen Guoheng Technology Co. Epichlorohydrin (EPI) was purchased from Guangzhou Jiangshun Chemical Co. Methylene blue (MB) was purchased from Tianjin Damao Chemical Reagent Factory in Tianjin, China. Hydrochloric acid (HCl), sodium hydroxide (NaOH), and anhydrous ethanol (CH_3CH_2OH) were purchased from Laiyang Kangtai Chemical Co. All other chemicals were of analytical purity and used during the experiments without further purification.

2.2 Preparation of GO/β-CD Composites

The in situ modification method was employed for the synthesis of GO/β-CD composites. 15 g of β-CD, 50 mL of NaOH solution (20% w/w), and 35 mL of epichlorohydrin were added to mixture beaker. Then, 2.25 g of graphene oxide was mixed in homogeneously and stirred at 70 °C until a paste was formed. The material was washed several times with deionized water until it reached a neutral pH. Additionally, residual epichlorohydrin in the synthetic material was eliminated through repeated washing. GO/β-CD composites obtained after vacuum freeze-drying were crushed and sieved with a 60-mesh sieve. The synthesis mechanism is shown in Fig. 1.

2.3 Characterization

Scanning electron microscopy (SEM) images of the GO and GO/β-CD composites were acquired using a cold-field emission scanning electron microscope (Model JSM-7500F). The adsorbent's surface functional groups were analysed using a Thermo Fisher Scientific Fourier transform infrared spectrometer (Nicolet iS5). The specific surface area was determined using Micro's Specific Surface and Porosity Analyser (ASAP 2460 3.01). GO/β-CD was also characterized using a Horiba Scientific confocal microscope Raman spectrometer (LabRAM HR model). The crystal structure of GO/β-CD was investigated using a PANalytical X-ray diffractometer (PANalytical X-pert).

2.4 Adsorption Experiments

First, the adsorption effects of the β-CD, GO, and GO/β-CD composites were compared under the same conditions. β-CD, GO, and GO/β-CD composites weighing 0.01 g each were added to 50 mL of a 100 mg/L methylene blue solution. The composites were then placed in a thermostatic water bath shaking chamber at 25 °C and 180 r/min for 30 min. The supernatants were centrifuged, and the absorbance values were measured at the maximum absorption wavelength of 664 nm. The concentration of MB was

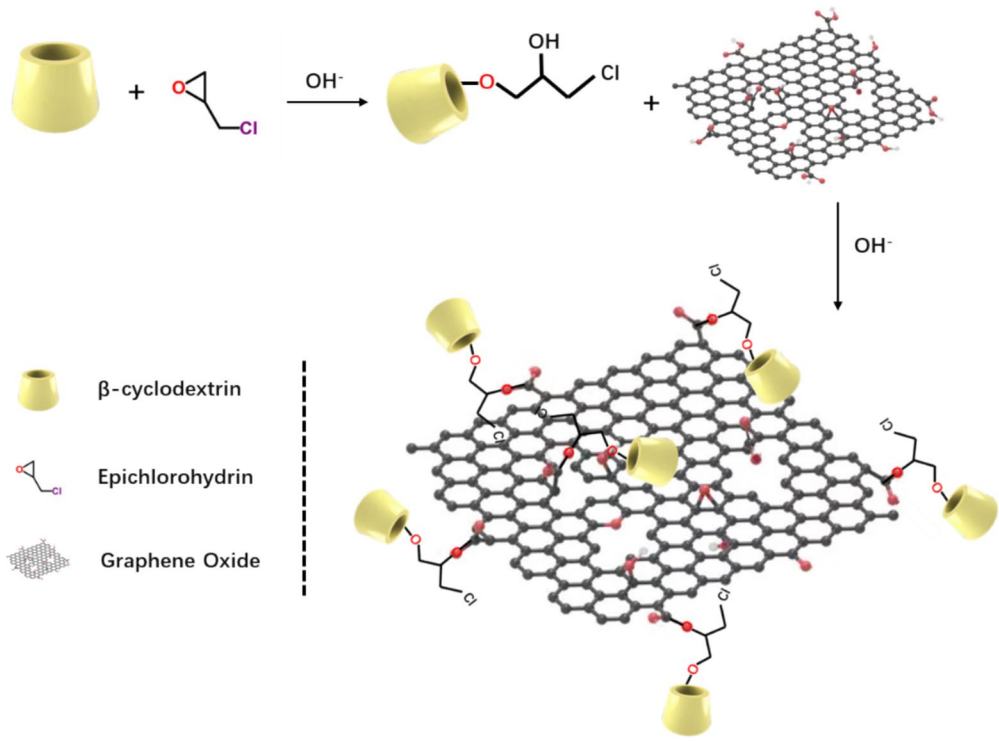

Fig. 1 Schematic diagram displaying the main steps used for β-CD/GO synthesis

determined based on the calibration curve (Figure S1).

In addition to the type of adsorbent, various parameters directly influence the adsorption performance of MB. The optimal adsorption conditions for this adsorbent were determined by varying one factor while keeping the others constant. These factors included the adsorbent dosage (0.0030 g, 0.0060 g, 0.0090 g, 0.0120 g, 0.0150 g, 0.0180 g, 0.0200 g, 0.0400 g, 0.0600 g), the pH of the MB solution (2, 4, 6, 8, 10, 12), temperature (20 °C, 30 °C, 40 °C, 50 °C, 60 °C, 70 °C), initial MB concentration (100 mg/L, 150 mg/L, 200 mg/L), and contact time (30 s, 1 min, 5 min, 10 min, 30 min, 40 min, 60 min).

2.5 Adsorption Isotherm Studies

2.5.1 Langmuir Adsorption Isotherm

The Langmuir isothermal adsorption model is based on two fundamental assumptions. First, it is assumed that the surface of the adsorbent is homogeneous. Second, the adsorption energy at each adsorption site is assumed to be identical. Additionally, the model assumes that the adsorption process occurs in a monolayer. After a film of adsorbed molecules forms on the surface of the adsorbent, the adsorption capacity of the adsorbent reaches an equilibrium where the adsorption rate of the adsorbent is equal to the desorption rate. On the surface of the adsorbent, there is no adsorption transfer phenomenon between the adsorption sites. In other words, each adsorption site can contain only one adsorbate molecule (Zakaria et al., 2022; Zhao et al., 2021). The Langmuir isothermal adsorption model is shown in Eq. (1).

$$\frac{1}{q_e} = \frac{1}{q_{max}} + \frac{1}{C_e}\left(\frac{1}{q_{max}K_L}\right) \quad (1)$$

q_e Adsorption equilibrium capacity (mg/g)
q_{max} Theoretical maximum adsorption capacity (mg/g)
C_e Mass concentration at adsorption equilibrium (mg/L)
K_L Langmuir adsorption parameters

2.5.2 Freundlich Adsorption Isotherms

The Freundlich isothermal isotherms (Eq. 2) is an empirical equation that reflects the reversibility of adsorption and the infinite nature of the adsorption process. The relationship between the amount of adsorption obtained on a nonuniform surface and the heat of adsorption, as derived from adsorption theory, aligns well with the Freundlich adsorption isotherm (Gunes et al., 2021).

$$\ln q_e = \ln K_F + \frac{1}{n}\ln C_e \quad (2)$$

K_F, 1/nFreundlich adsorption parameters

2.5.3 Temkin Isothermal Adsorption

The Temkin isotherm reflects both the type of adsorbent and the interactions between adsorbates. This model assumes that; (1) interactions between the adsorbent and adsorbent mass result in a linear decrease in the heat of adsorption and in the coating of all the molecules on the adsorbent surface, and (2) the surface binding energy of the adsorbent is homogeneous and maximized. The isothermal adsorption model can be expressed by the following Eq. (3) and Eq. (4) (Javed et al., 2021; Nayak et al., 2022):

$$q_e = B_1 \ln K_T + B_1 \ln C_e \quad (3)$$

$$B_1 = \frac{RT}{b} \quad (4)$$

K_T the Temkin constant (L/mol)
B_1 The Temkin constant related to the heat of adsorption (J/mol)
R ideal gas constant, 8.314 J/(mol-K)
T the absolute temperature (K)

2.5.4 Dubinin–Radushkevich Isothermal Adsorption

Based on the study of the adsorption mechanism, Dubinin et al. proposed the use of the adsorption potential and introduced a new theory of microporous filling. The adsorption potential refers to the amount of work required to attract 1 mol of gas from the main phase to the adsorbed phase. The molecular-level adsorption mechanism on a microporous adsorbent is theoretically distinct from that on a surface due to the close arrangement of the pore walls and the overlap of adsorption potentials. The Dubinin–Radushkevich adsorption theory suggests that the adsorption surface is nonhomogeneous. The outcome of this equation determines whether the adsorption process is physical or chemical (A. Wang et al., 2021). The Dubinin–Radushkevich isothermal adsorption model is expressed as in Eq. (5), Eq. (6), Eq. (7) (Toan et al., 2023):

$$\ln Q_e = \ln Q_m - K_D \varepsilon^2 \quad (5)$$

$$\varepsilon = RT\ln\left(1 + \frac{1}{C_e}\right) \quad (6)$$

$$E = \frac{1}{\sqrt{2K}} \quad (7)$$

K_D Adsorption constant related to the mean free energy of the adsorption process (mol^2/kJ^2)
M Saturated (monolayer) adsorption capacity (mol/g)
ε adsorption potential
T Adsorption reaction temperature (K)

E represents the free energy of adsorption, and the adsorption characteristics can be determined based on its magnitude. When the energy (E) is between 8 and 16 kJ/mol, the process is an ion exchange. An E less than 8 kJ/mol is considered as physisorption, while E greater than 16 kJ/mol indicates the reaction is chemisorption.

2.6 Adsorption Kinetics

2.6.1 First Order Kinetic Model

Lagergren's first-order rate equation, which is based on the amount of solid adsorbed, is the most used equation. The basic assumption of the first-order kinetic equation is that the diffusion step determines the adsorption process. It also assumes that there is a direct relationship between the rate of adsorption and the difference between the amount of adsorbed substance and the equilibrium amount at any given moment (S. Yang et al., 2019a, 2019b).

The expression for the first-order kinetic equation is shown in Eq. (8) (Habila et al., 2022).

$$\ln(q_e - q_t) = \ln q_e - \frac{k_I}{2.303}t \quad (8)$$

k_1 Quasiprimary kinetic rate parameter (min^{-1})
q_e Adsorption of MB by GO/β-CD at equilibrium (mg/g)
q_t Adsorption of GO/β-CD on MB at time t (mg/g)

2.6.2 Second Order Kinetic Model

The second order kinetic model suggests that the efficiency of adsorption is determined by the processes of electron sharing and transfer between the adsorbent and adsorbate. The basic assumption of the second order reaction kinetic equation is that the rate of adsorption is determined by the square of the number of adsorbed vacancies on the adsorbent surface in the unoccupied state (Bucur et al., 2021; Rajendran et al., 2022). The second order reaction kinetic equation is shown in Eq. (9).

$$\frac{t}{q_t} = \frac{1}{k_2 q_e^2} + \frac{1}{q_e}t \quad (9)$$

$k_2$second order kinetic rate parameter (min^{-1})

2.6.3 Kinetic Equation for Intraparticle Diffusion

The kinetic equation for intraparticle diffusion assumes that the resistance of liquid film diffusion is negligible or has only a minor impact during the initial phase of adsorption. It is primarily concentrated at the boundaries of the adsorbent particles. The diffusion behaviour of particles in water is the main controlling factor for the adsorption behaviour of pollutants, regardless of the adsorption time and location. Adsorption of an adsorbent from the liquid phase to the solid phase is a reversible reaction that reaches two-phase equilibrium (Lin et al., 2019). The kinetic equation for intraparticle diffusion is shown in Eq. (10) (L. Zhu et al., 2019).

$$q_t = k_{id}t^{0.5} + C \quad (10)$$

k_{id} the intraparticle diffusion parameter
C boundary layer constant

2.6.4 Bangham Model

The Bangham model (Eq. 11) is now commonly used to describe the mechanisms of pore diffusion. If the kinetic experimental data are fitted with this equation as a straight line and the line passes through the origin, the diffusion is controlled by internal diffusion. Conversely, a weak linear relationship would indicate that adsorbate diffusion within the pore is not the only step limiting the velocity. Membrane diffusion and intrapore diffusion play important roles in all stages of adsorption separation (Rezakazemi & Shirazian, 2019; Zghal et al., 2023).

$$\log\log\left[\frac{C_0}{C_0 - q_t m}\right] = \log\left[\frac{k_0 m}{2.303}\right] + \alpha \log t \quad (11)$$

q_e t juncture (min) adsorption capacity per unit mass of adsorbent (mg/g)
m concentration of adsorbent in solution (g/L)

2.7 Thermodynamic Study of Adsorption

The change in the thermodynamic parameter Gibbs free energy for the adsorption reaction was calculated according to the following Eq. (12), (13), (14) (Parimelazhagan et al., 2022).

$$\ln K_c = -\frac{\Delta H}{RT} + \frac{\Delta S}{R} \quad (12)$$

$$K_c = \frac{C_{Ae}}{C_e} \quad (13)$$

$$\Delta G = -RT\ln K_c \quad (14)$$

ΔG Gibbs free energy of the adsorption process (kJ/mol)
ΔH free braizing variation in the adsorption process (kJ/mol)
ΔS the first change in the adsorption process, J/(mol·K)
K_c equilibrium constant (L/g)

R ideal gas constant, assumed to be 8.314 J/(mol·K)
T the absolute temperature (K)

2.8 Regeneration

For regeneration and recovery analyses, 50 mg/g of adsorbent was initially added to a solution of MB (25 mg/g) and stirred at 25 °C for 24 h. Once saturated, the adsorbent was regenerated by immersing it in 50 mL of desorbent (varied between ionized water, anhydrous ethanol, hydrochloric acid solution, or sodium hydroxide) for 6 h. The desorbent was extracted using a filtered syringe to obtain the absorbance value. The concentration of MB in the desorbent was calculated and compared with the other desorbents. Higher concentration of MB in the desorbent means more MB could be recovered. The desorbent with the best desorption effect was then selected to study its regeneration capacity. The regenerated adsorbent was separated and washed with deionized water for reuse. About six adsorption–desorption cycles were studied for this purpose.

3 Results and Discussion

3.1 Characterization and Analysis of GO/β-CD Composites

The morphology and structure of the graphene oxide (GO) and GO/β-CD composites were observed using scanning electron microscopy, as depicted in Fig. 2. GO exhibits a typical lamellar fold structure (Fan et al., 2020), which is dense and possesses a relatively smooth surface. The GO/β-CD composite still retain some of the GO folds but was significantly reduced. The folds are present in graphene oxide to maintain stability, while the folds are weakened in GO/β-CD, indicating that GO/β-CD is more stable than graphene oxide (Jun Wang et al., 2014). GO/β-CD has a porous sponge-like shape, and the surface has been successfully incorporated with crystals of β-CD, which have an irregular blocky shape. β-CD cross-linking increased the distance between the graphene oxide layers, which theoretically had a positive adsorption effect. The nitrogen adsorption and desorption isotherms of the GO/β-CD composites are shown in Fig. S2. The results indicate that the adsorption of GO/β-CD composites is a type II adsorption as a monolayer macroporous adsorption, which is consistent with the average pore size of 95 nm (Table S1). The specific surface area can reach up to 0.25 m^2/g. A high specific surface area provides more active sites for capturing and immobilizing MB. Furthermore, an increased number of active sites facilitates greater contact with and adsorption of target molecules, reduces diffusion limitations, and accelerates the adsorption process.

Figure 3 shows a prominent diffraction peak near 2θ of 8.85° for the crystalline surface of graphene oxide (001), suggesting that the graphene oxide was not fully reduced during the material synthesis. The XRD peaks of graphene oxide are relatively sharp, indicating a shorter-ordered structure and thinner thickness. The characteristic diffraction peaks of β-CD appeared at 2θ values of 13.62°, 17.83°, and 20.60° (Tene et al., 2022). The peak at 2θ of 42.40° is attributed to the insertion of cyclodextrin derivatives into the intermediate layer of graphene oxide. A β-CD molecule contains seven reactive hydroxyl groups that can react simultaneously with the epoxy groups on the surface or edges of the graphene oxide molecule. The reaction results in an expansion of the spacing within the intermediate layer. Ultimately, the bonding of graphene oxide nanoparticles results in the formation of a complex, long-range, ordered structure at various angles (Z. Yang et al., 2021).

Raman analysis is a highly effective technique for characterizing carbon materials. The GO and GO/β-CD composites were analysed using Raman spectroscopy. Both the GO and GO/β-CD composites in Fig. 4 exhibit obvious D and G characteristic peaks. The D and G peaks are both Raman characteristic peaks of carbon atoms. The former represents the defects and disorder of the carbon atom crystals in the sp^3 orbitals, which usually appear near 1350 cm^{-1}; the latter represents the vibrational defects and disorder of the carbon atoms in the sp^2 orbitals, which usually appear near 1600 cm^{-1} (De Figueiredo Neves et al., 2020). The D/G intensity ratio (I_D/I_G), which characterizes the ratio of sp^2/sp^3 carbon atoms, is an important factor in determining the degree of disorder in graphite(Borandeh et al., 2021). The I_D/I_G value of GO is 1.15, while that of GO/β-CD is 1.23. These results indicate that GO/β-CD has more structural

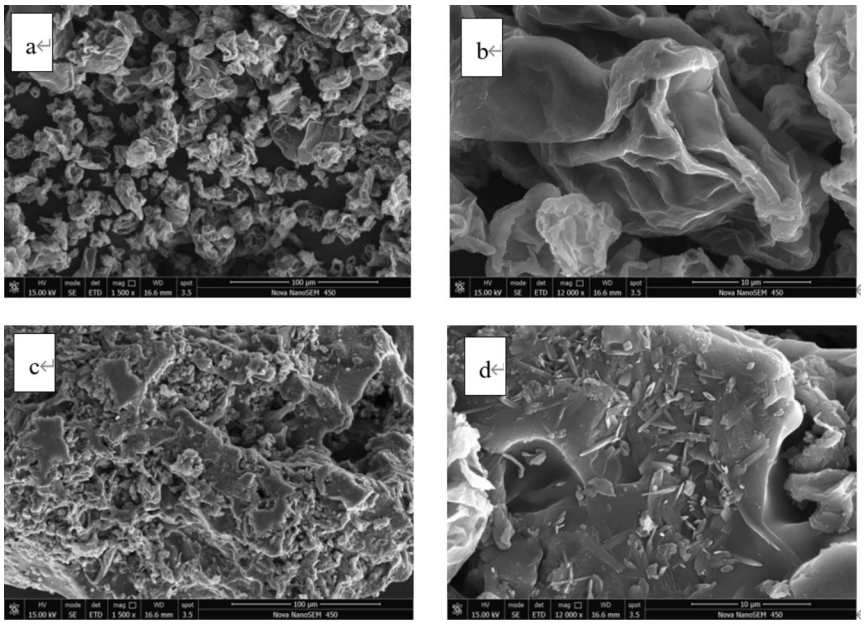

Fig. 2 SEM images for; (a) GO (magnified 1,500 times); (b) GO (magnified 12,000 times); (c) GO/β-CD (magnified 1,500 times); (d) GO/β-CD e (magnified 12,000 times)

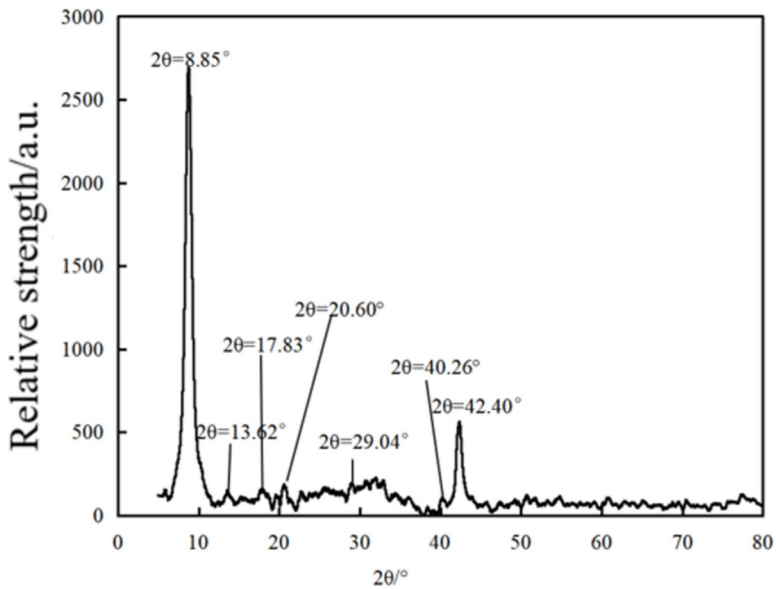

Fig. 3 GO/β-CD composite XRD pattern

defects than GO. In addition, Raman spectral analysis of GO/β-CD showed a blueshift (~4 cm^{-1}) in the G-band compared to that of GO, which may be attributed to the reduction in the number of graphene layers (Ferrari, 2007).

The changes in the surface functional groups of graphene oxide (GO), beta-cyclodextrin (β-CD), and GO/β-CD were analysed using FT-IR spectroscopy. As shown in Fig. 5, 1060 cm^{-1} represents the C-O stretching vibration in the epoxy group, 1733 cm^{-1} corresponds to the C=O stretching vibration in the carboxyl group, and the peak at 3396 cm^{-1} corresponds to the stretching vibration of -OH (Al-Yaari & Saleh, 2023). In the FT-IR spectrum of β-CD, the peak at 950 cm^{-1} corresponds to the α-1,4-glucose bond, the peak at 1055 cm^{-1} corresponds to the C-O stretching vibration, and the peak at 1661 cm^{-1} corresponds to the C=O stretching vibration (G. Zhu et al., 2021). Comparison between the FTIR

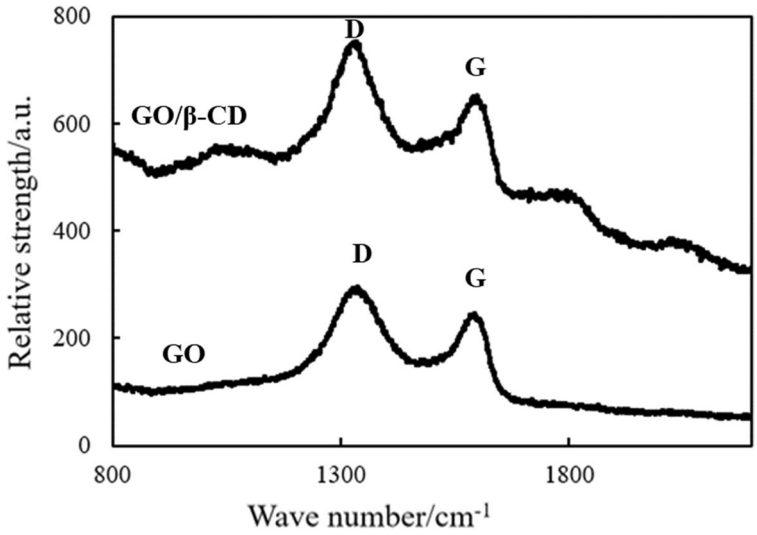

Fig. 4 Raman diagram of GO and the GO/β-CD composites

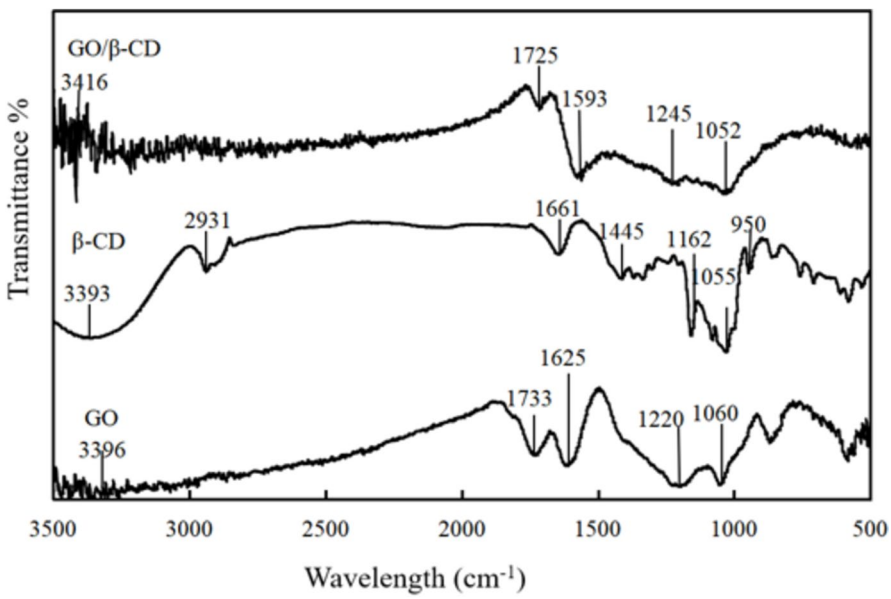

Fig. 5 FT-IR diagram of GO, β-CD, and the GO/β-CD composite

spectra revealed the characteristic peaks of both GO and β-CD at 1052 cm^{-1} and 1725 cm^{-1} were notably reduced. This suggests that β-CD was primarily attached to the surface of GO through reactions involving carboxyl and epoxy groups, resulting in the creation of active carboxyl group sites. Therefore, abundant hydroxyl groups were observed on the surface of the composite. It was reported that the ionization of hydroxyl groups produces hydrogen ions, which readily combine with the cations of MB (C. Fu et al., 2019). Therefore, GO/β-CD could strongly adsorbs MB.

3.2 Optimisation of Adsorption Conditions for GO/β-CD Composites

3.2.1 Adsorption Capacity of β-CD, GO and GO/β-CD Composites

As shown in Fig. 6, the MB adsorption capacities of pure β-CD and GO were 15.39 mg/g and 215.35 mg/g, respectively. In contrast, the adsorption capacity of the GO/β-CD composite reached 401.84 mg/g, which was significantly greater than the previously reported

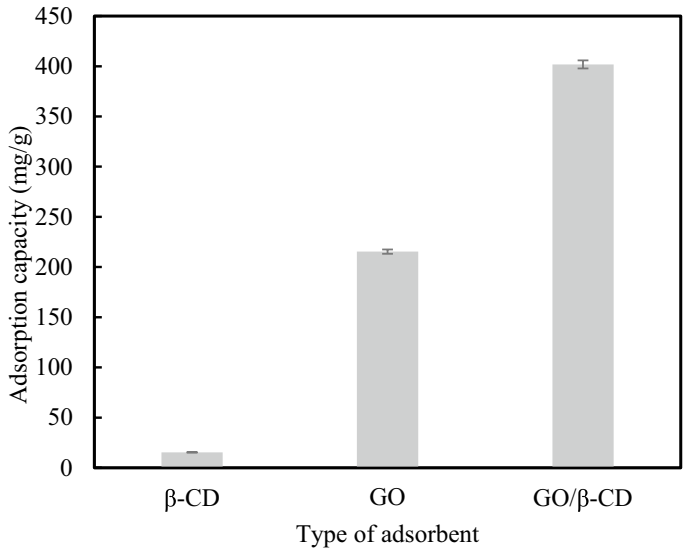

Fig. 6 Comparison of the MB adsorption by β-CD, GO and GO/β-CD composites at 0.2 g/L GO/β-CD composites, pH = 6, 25℃, 30 min and 100 mg/L MB concentration

composites (Jawad et al., 2021; Usman et al., 2021). GO adsorption occurs mainly through abundant functional groups that enhanced its adsorption effectiveness (Zainal et al., 2021). After composite formation, the GO/β-CD composite exhibited numerous cavities and folded structures, resulting in a larger specific surface area (Table S1). It retains the original abundant functional groups of GO and introduces a significant number of effective carboxylate active sites during the reaction process. Consequently, the composite material demonstrates enhanced adsorption of MB due to the abundance of functional groups and effective adsorption sites.

3.2.2 Effects of GO/β-CD Composite Dosage on the Adsorption Performance

As shown in Fig. 7, with increasing dosage, the removal of MB by the GO/β-CD composites initially increased and then stabilized, while the adsorption amount continuously decreased. This is because the increase in the amount of GO/β-CD composite provides more total amount of active sites, leading to an increased removal rate. However, the amount of MB that could be removed was limited, resulting in a plateau in the removal rate. The adsorption capacity exhibited an inverse trend with the dosing amount, attributed to the abundance of active sites and the substantial adsorption capacity that remained underutilized in low concentrations of the MB solution (Dong et al., 2023). Therefore, a GO/β-CD composite dose of 0.012 g was selected for the subsequent experiments.

3.2.3 Effects of pH on the Adsorption Performance

The MB adsorption by GO/β-CD composites was influenced by pH, as depicted in Fig. 8. When the pH increased from 2 to 6, the removal rate increased from 64.41% to 95.39%, and the adsorption amount increased from 268.39 mg/g to 397.45 mg/g. Subsequently, as the pH continued to increase up to pH 12, the removal rate and adsorption capacity of MB remained unchanged. The relatively low removal of methylene blue (MB) by GO/β-CD in acidic environment may be attributed to the competition between H^+ ions in the solution and MB for the adsorption sites. At the same time, the hydroxyl and carboxyl groups in the GO/β-CD composites were protonated, leading to electrostatic repulsion with the cationic dye MB, resulting in decreased adsorption performance. After the increase in pH, the hydroxyl and carboxyl groups were deprotonated, leading to the disappearance of cationic electrostatic repulsion with MB (Jawad et al., 2021). Therefore, GO/β-CD composites were more effective at adsorbing MB in neutral to alkaline environments.

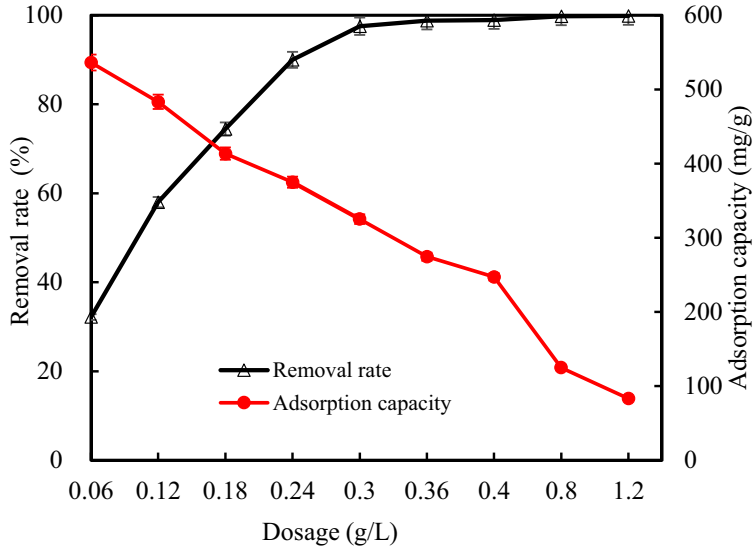

Fig. 7 Effect of dosage of the GO/β-CD composite on the MB adsorption at pH = 6, 25℃, 30 min and 100 mg/L MB concentration

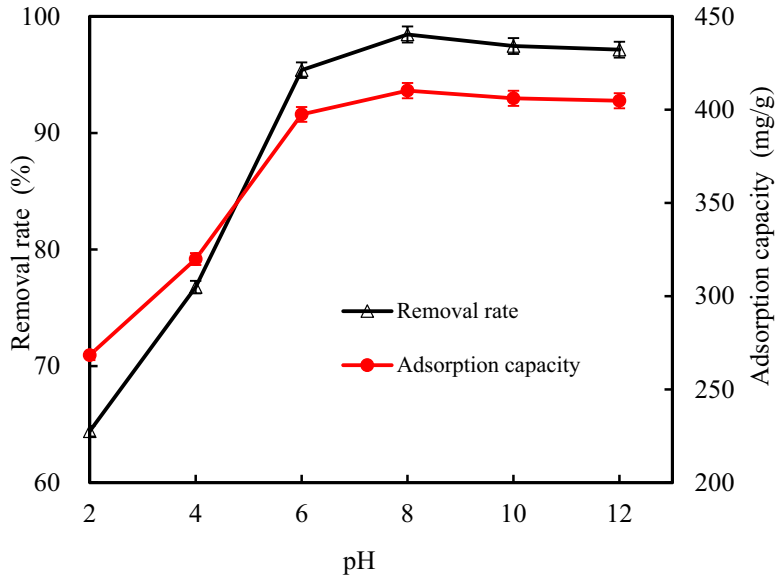

Fig. 8 Effect of pH on the MB adsorption of the GO/β-CD composites at 0.2 g/L GO/β-CD composites, 25℃, 30 min and 100 mg/L MB concentration

3.2.4 Effects of Temperature on the Adsorption Performance

The effect of temperature on the adsorption of MB dye by GO/β-CD composites is shown in Fig. 9. With increasing temperature, the removal rate and adsorption capacity initially increased and then remained unchanged. When the temperature increased from 20 °C to 40 °C, the removal rate of MB by GO/β-CD composites increased from 81.47% to 97.13%, and the adsorption capacity increased from 339.46 mg/g to 404.71 mg/g. Thereafter, the removal rate and adsorption capacity remained basically unchanged. The experimental results showed that the process of MB adsorption by GO/β-CD composites is a heat absorption process (Dong et al., 2023).

3.2.5 Effects of Initial MB Concentration and time on Adsorption Performance

As shown in Fig. 10, with increasing initial concentration of MB and the contact time, the removal percentage increased. The removal rate and adsorption amount of MB by the GO/β-CD composites increased

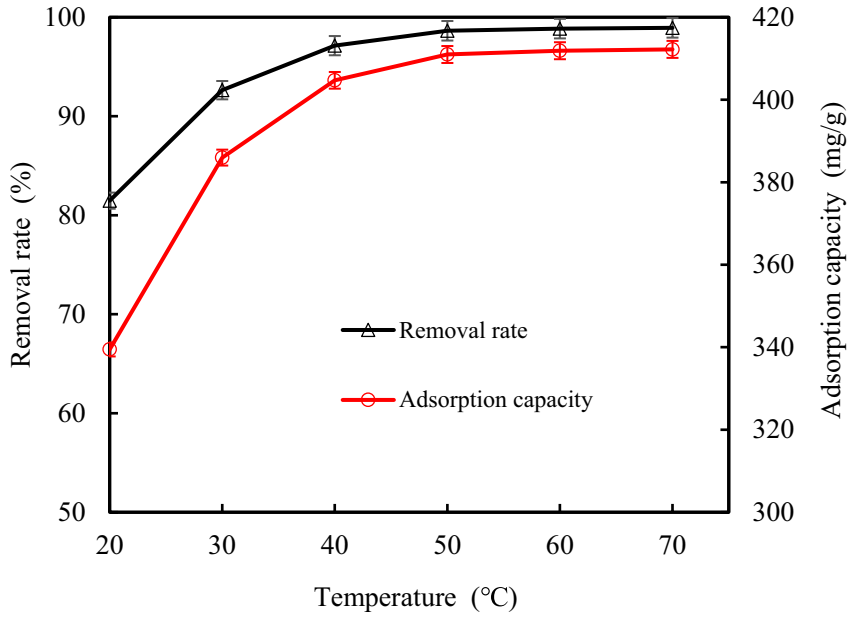

Fig. 9 Effect of temperature on the MB adsorption of the GO/β-CD composites at 0.2 g/L GO/β-CD composites, pH = 6, 30 min and 100 mg/L MB concentration

gradually and finally stabilized. However, at high initial concentration of MB, the increasing trend of the removal rate with time was not distinct especially after 30 min. This implies that the adsorption sites of the GO/β-CD composites were specific, and the adsorption capacity of MB was restricted. When the initial concentration of the dyes increased, more molecules could be adsorbed on the composite material, leading to the establishment of equilibrium faster (Xu et al., 2022). Therefore, the equilibrium time for high concentration MB adsorption over GO/β-CD composites was 30 min, while the adsorption saturation capacity of the GO/β-CD composites was approximately 450 mg/g.

3.3 Adsorption Isotherm

The fitting of the adsorption experiments conducted at 25 °C with the Langmuir, Freundlich, Temkin, and Dubinin−Radushkevich adsorption isotherms are depicted in Fig. 11, and the corresponding parameters are listed in Table 1.

From Table 1, the Langmuir-type adsorption isotherm is considered as the most ideal adsorption model for GO/β-CD composites on MB due to the highest fitting correlation coefficient (R^2). Hence, the adsorption process could be taken as monomolecular layer adsorption. After the adsorbent adsorbs MB molecules, the MB molecules do not undergo any transfer or movement between the adsorption sites, and there is no mutual interaction between the MB molecules. The theoretical maximum adsorption capacity of the composite was calculated using the Langmuir model to be 434.78 mg/g, which significantly surpassed the adsorption capacities of MB by other adsorbents documented in the literature (Table 2). This exceptional performance can be attributed to the carboxylate active sites created by the epoxy carboxylation reaction of GO combined with β-CD, as well as the numerous functional groups present in the composite that enable it to adsorb a substantial quantity of MB. Although the Freundlich model is not strongly correlated as compared to the Langmuir model, it is worth mentioning the parameters associated with its adsorption mechanism. The parameter n reflects the difficulty of the adsorption reaction. When n equals to 3.79, which is greater than 1, the adsorption reaction proceeds smoothly under the given conditions. Moreover, the free energy of adsorption of the composites based on the Dubinin−Radushkevich (D-R) model was calculated to be greater than 16 kJ/mol, indicating a chemisorption process.

3.4 Adsorption Kinetics

Kinetic models were fitted to the adsorption data, and the results and related parameters obtained are shown in Fig. 12 and Table 3.

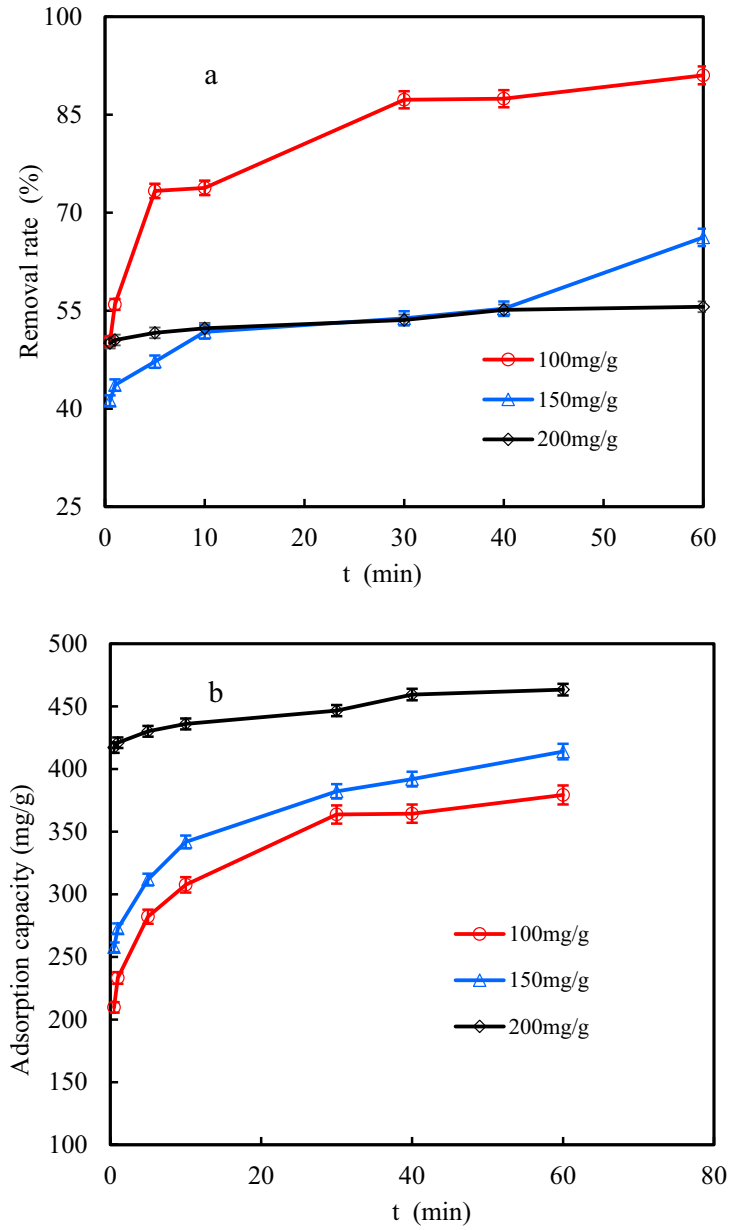

Fig. 10 Effect of contact time and initial concentration of MB at 0.2 g/L GO/β-CD composites, pH = 6, 25℃(**a**) removal rate; and (**b**) adsorption capacity

Table 3 shows that the second kinetic model MB by GO/β-CD composites gave the best fitting $R^2 = 0.9988$, indicating a significant correlation. This means, the adsorption of MB by GO/β-CD composites involves chemical adsorption as the primary process, accompanied by physical adsorption. The internal diffusion curve consists of three parts. In the first stage, the adsorption reaction occurred rapidly, transferring the adsorbate from the liquid phase to the surface of the GO/β-CD composite due to the boundary layer diffusion, a process also referred to as surface mass transfer. The second segment reflects the macropore diffusion process within the particles, and the third segment (30 ~ 60 min) reflects the diffusion of the adsorbate within the mesopores and micropores. As the second segment lasts longer than the first one, it can be said that the diffusion of the adsorbent within the particles was dominated by macroporous diffusion, which was consistent with the conclusion obtained from the BET characterization. The fit to

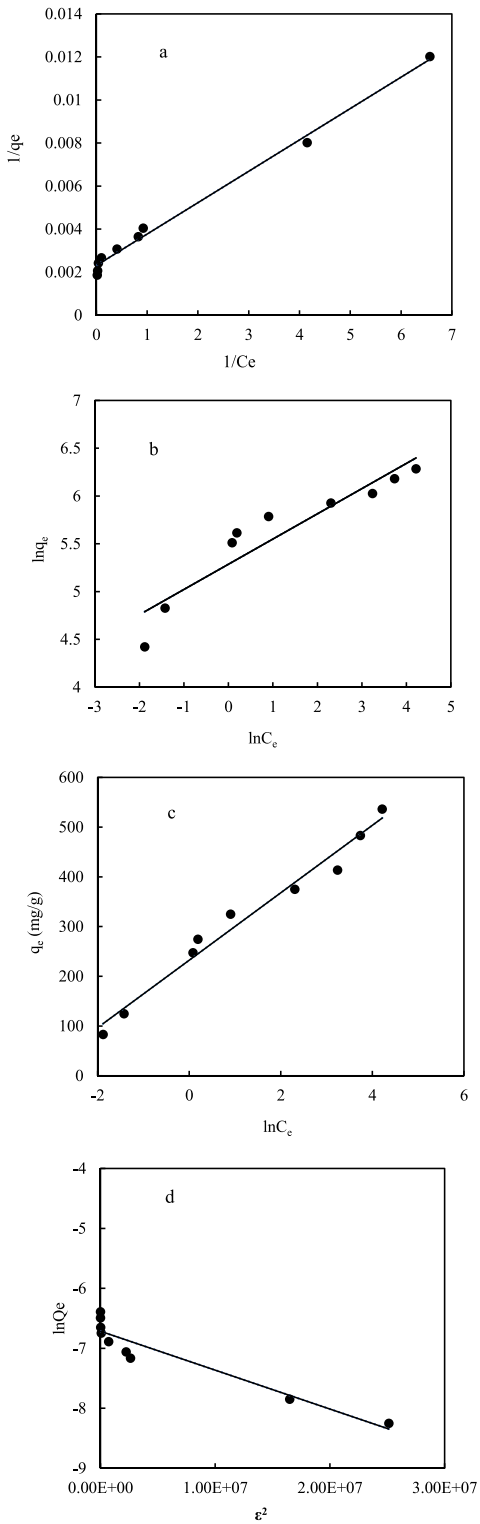

Fig. 11 (**a**) Langmuir-type adsorption isotherm model fit; (**b**) Freundlich-type adsorption isotherm model fit; (**c**) Temkin-type adsorption isotherm model fit; (**d**) Dubinin−Radushkevich-type adsorption isotherm model fit

Bangham's model equation is also high, $R^2 = 0.9855$, indicating a good fit, but the fit line did not pass through the origin. This suggests that the adsorption of MB by the GO/β-CD composites was primarily controlled by macroporous diffusion.

3.5 Adsorption Thermodynamic

The thermodynamic model fitting and related parameters for the adsorption of MB by GO/β-CD composites are shown in Fig. S3 and Table 4. Analysis of Fig. S5 and Table 4 reveals that the ΔG value for the MB dye adsorbed by the GO/β-CD composites is negative, indicating that the reaction occurs spontaneously. As the temperature increases, the absolute value of ΔG increases, leading to a greater tendency for the reaction to proceed spontaneously. A positive value of the reaction entropy ΔS indicates an increase in the degree of disorder at the solid−liquid interface during the adsorption of MB by GO/β-CD composites. A positive value of ΔH indicates that the adsorption of MB by GO/β-CD composites is an endothermic reaction.

3.6 Adsorption Mechanism

To promote the generation of stable polymers with superior porosity and adsorbed three-dimensional structures, a new preparation technique was applied. The β-CD polymer obtained by using epichlorohydrin as a cross-linking agent under alkaline conditions overcame the disadvantage of β-CD's susceptibility to water solubility. By utilizing an esterification reaction, the cyclodextrin polymer was loaded onto graphene oxide to address the technical challenge of spatial collapse resulting from the interweaving of polymer molecular chains. This process led to the formation of a microporous structure with a high specific surface area. The large number of pores provided abundant active sites and channels, which promoted the adsorption of β-CD/GO on MB (refer to Fig. 1c and 1d). Furthermore, as shown by FTIR (Fig. 4), the surface of β-CD/GO is covered in a great deal of carboxyl groups. One of the most important variables in the cationic dye adsorption process is the electrostatic interaction between the -COOH group of β-CD/GO and the cationic dye molecules (C. Fu et al., 2019). According to earlier research (X. Liu et al., 2019; Jingjing Wang et al., 2019), there is a good chance

Table 1 Adsorption Isotherm Model Parameters

Adsorption isotherm model	Parametric	Value
Langmuir	adsorption isotherm equation	y = 0.0015x + 0.0023
	q_{max} (mg/g)	434.7826
	K_l (L/mg)	3.45E-06
	R^2	0.9927
Freundlich	adsorption isotherm equation	y = 0.2637x + 5.2859
	K_F (mg/g-(1/mg)$^{1/n}$)	197.5319
	n	3.7922
	R^2	0.8832
Temkin	adsorption isotherm equation	y = 67.821x + 232.35
	K_T (L/mol)	30.7503
	B_1	67.8210
	R^2	0.9758
Dubinin−Radushkevich	adsorption isotherm equation	y = -6E-08x-6.7158
	Q_m (mol/g)	1.21E-03
	K_D (mol^2/g)	6E-08
	R^2	0.9014
	E (kJ/mol)	2886.8360

Table 2 Comparison of Maximum Monolayer Capacity for MB on the Other Adsorbents

Adsorbents	Q_m (mg/g)	References
Nitrilotriacetic acid β-Cyclodextrin-Chitosan (NTA-β-CD-CS)	163	(Usman et al., 2021)
Dragon Fruit Peel Activated Carbon (DFPAC)	195	(Jawad et al., 2021)
Magnetic activated carbon (MACz)	156	(Yağmur & Kaya, 2021)
Magnetic alginate/rice husk	274	(Alver et al., 2020)
Carbon nanotubes-based polymer nanocomposites	189	(Gan et al., 2020)
GO/β-CD	435	This study

that β-CD/GO and cationic dye molecules will interact through hydrogen bonding and π-π interactions. As MB molecules approach the surface of GO, the interaction between the conjugated π-electron systems of MB and the unperturbed graphene regions on GO facilitates π-π conjugation. This interaction promotes the planar alignment of MB molecules on the GO surface, allowing for π-electron cloud overlap and consequently enhancing intermolecular stability. Furthermore, the hydroxyl (-OH) and carboxyl (-COOH) groups on the GO surface can function as hydrogen bond donors, while the nitrogen atoms in MB serve as hydrogen bond acceptors. Thus, as MB molecules approach the GO surface, hydrogen bonding interactions between the -OH or -COOH groups of GO and the nitrogen atoms of MB are established, thereby augmenting the adsorption capacity of MB on the GO surface. Lastly, β-CD's distinct qualities enable it to encapsulate organic dye impurities and create distinct "host–guest" complexes because of its hydrophobic and nonpolar inner cavity (Alsbaiee et al., 2016; Qu et al., 2020). To create encapsulated complexes, the β-CD component of β-CD/GO can thus use "host–guest" supramolecular interactions to trap MB organic molecules as "guest" substances in its inner cavity. This phenomenon conforms with additional reports found in the literature (Chen et al., 2020; Ozelcaglayan & Parker, 2023).

3.7 Analysis of the Number of Recycling Cycles for the Adsorption of MB

From an economic perspective, the recovery and the reuse of adsorbents are crucial stages of the adsorption

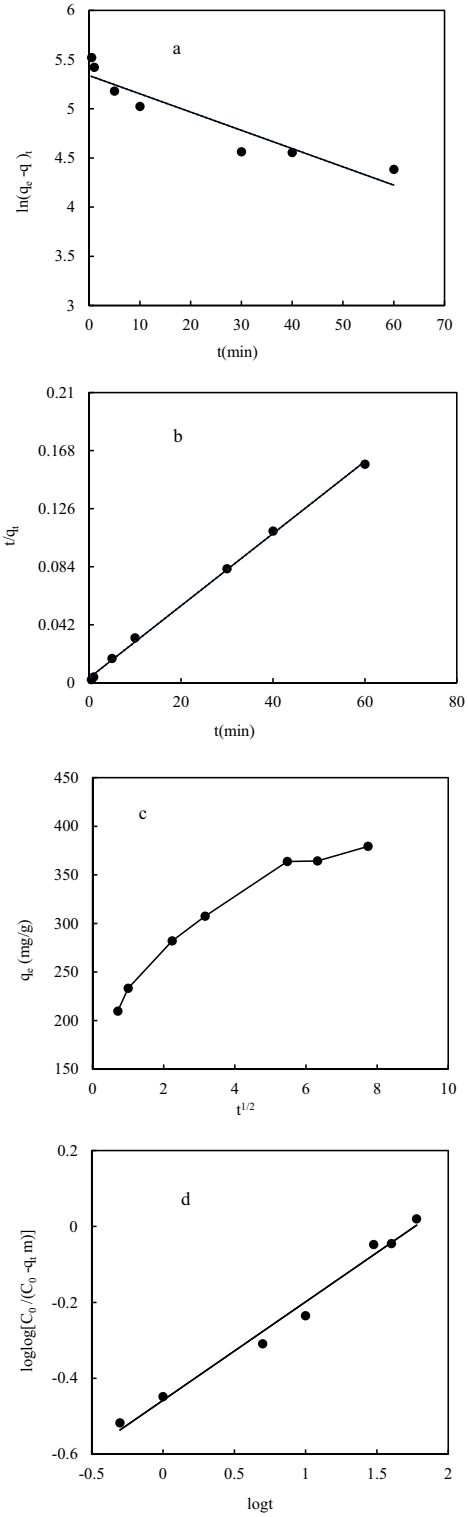

Fig. 12 Adsorption kinetic model fitting; (**a**) Fitting of the quasiprimary kinetic model for GO/β-CD adsorption of MB; (**b**) Fitting of the quasisecondary kinetic model for GO/β-CD adsorption of MB; (**c**) Fitting of the intraparticle diffusion model for GO/β-CD adsorption of MB; (**d**) Fitting of the GO/β-CD adsorption of MB

method. Therefore, the adsorbents in the system should be properly processed to facilitate the recovery of GO/β-CD. As seen from Fig. 13, the desorption capacity of the four desorbents are decreasing in the following order: ethanol > HCl > water > NaOH. Desorption of water is ineffective due to the chemisorption of GO/β-CD on MB. Moreover, the adsorption of GO/β-CD on MB is not ion exchange but is dominated by chemical bonding forces, as discussed in Sect. 3.3. Therefore, the desorption effect of ethanol is better, while the desorption effect of acid−base solution is worse (Dai et al., 2021). Moreover, ethanol was more readily available and less toxic, so ethanol was selected as the desorption agent for subsequent desorption experiments.

The GO/β-CD composite can be recycled, and the removal rate of MB decreased from 88.39% to 69.30% after five cycles of adsorption and desorption as shown in Fig. 14. This is because the adsorption of MB by GO/β-CD occurs via chemisorption. During the desorption process, ethanol breaks the binding bond between the GO/β-CD groups and the cationic dye MB. The dye molecules are not completely desorbed during the desorption process, leaving some residue. Additionally, there is a loss of composite material in the process of desorption and recycling, leading to a decrease in the efficiency of adsorption (H. Yang et al., 2019a, 2019b). However, the significant regeneration performance of the adsorbent and contaminants must be determined by a stable adsorption–desorption process. Therefore, the adsorption–desorption of the GO/β-CD composite was evaluated. As shown in Fig. 14, the removal performance of MB slightly decreased after six adsorption−desorption cycles. This suggests that GO/β-CD requires a proper regeneration step to restore the desired removal performance and has good reusability, making it a cost-effective and efficient adsorbent for the simultaneous treatment of wastewater. Moreover, the incorporation of graphene oxide improved the specific surface area of the adsorbent, increased the chemical

Table 3 Adsorption Kinetics Model Parameters

Adsorption kinetic modelling	Parameters	Value
quasiprimary kinetic model	Adsorption kinetic equation	y = -0.0186x + 5.3377
	K_1 (min^{-1})	0.04284
	q_e (mg/g)	208.0337
	R^2	0.8835
quasisecondary kinetic model	Adsorption kinetic equation	y = 0.0026x + 0.0036
	K_2 (g/(mg-min))	384.6154
	H (g/(mg-min))	1.88E-04
	R^2	0.9988
Intraparticle diffusion modelling	Adsorption kinetic equation	y = 23.801x + 215.06
	K_{id} (mg/(g-$min^{-0.5}$))	23.801
	C (mg/g)	215.06
	R^2	0.9358
Bangham model	Adsorption kinetic equation	y = 0.2594x-0.4579
	α	0.2594
	K_0 (mL/(g/L))	3.3433
	R^2	0.9855

Table 4 Adsorption Thermodynamic Modelling Parameters

T(K)	K_c	ΔG (KJ/mol)	ΔS (J/mol/k)	ΔH(KJ/mol)	Adsorption equation	R^2
293	4.3970	-3607.5301	6.7975	1.1482	y = -0.1381x + 0.8176	0.9188
303	12.5746	-6377.6587				
313	33.8419	-9164.4326				
323	72.1121	-11488.8300				
333	86.0572	-12,333.9775				
343	92.4211	-12,907.8165				

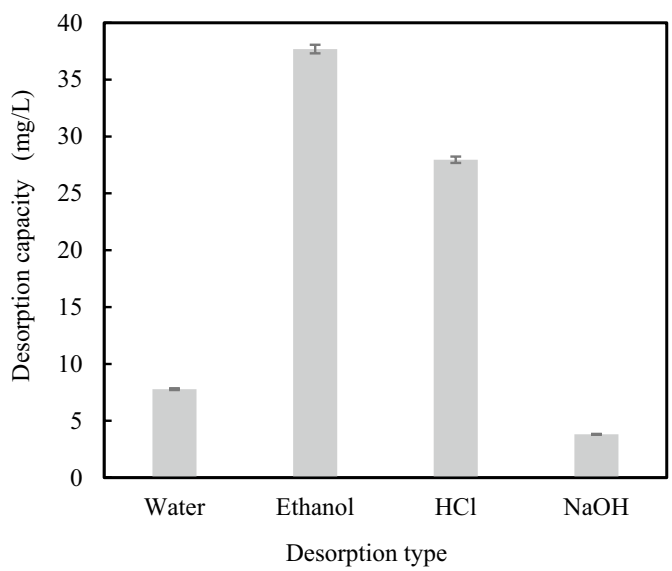

Fig. 13 MB desorption from composite materials by different desorbents at 0.2 g/L Adsorption-saturated GO/β-CD composites, pH = 6, 25℃, 30 h, HCl and NaOH 0.1 mol/L, Ethanol 99.5%

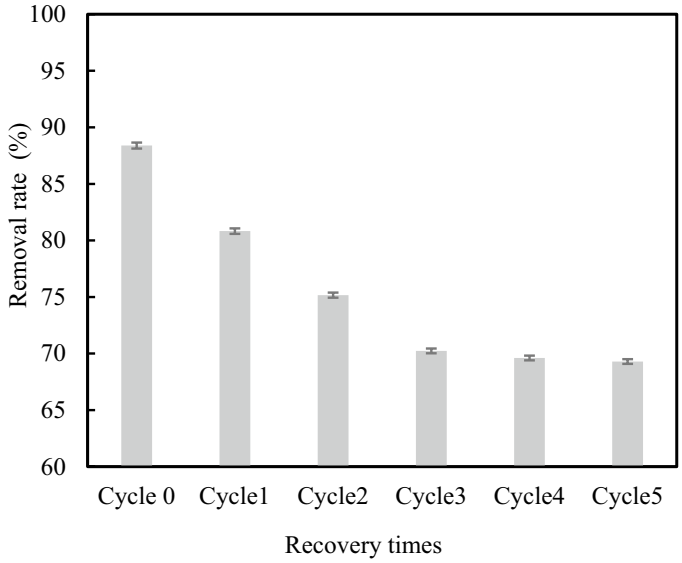

Fig. 14 Reuse of GO/β-CD composites for MB adsorption at 0.2 g/L GO/β-CD composites, pH = 6, 25℃, 30 min and 100 mg/L MB concentration

stability and hydrophobicity of the adsorbent, and facilitated the reuse of GO/β-CD composites.

4 Conclusion

I. In this study, ethylene oxide was used as a cross-linking agent to synthesize GO/β-CD composites. The composites were characterized by SEM, BET, FTIR, XRD, and Raman spectroscopy, which revealed that the materials had numerous pores and folds and that β-CD was successfully attached to the surface of GO. The adsorption process of the composites was primarily influenced by the adsorption of monomolecular layers of macropores. GO/β-CD exhibited a significant number of functional groups on its surface, and a considerable amount of effective carboxylate active sites were introduced. The composites possessed a rich array of adsorption sites, with multiple pores and defects, displaying a disordered and intertwined state. The defects present a messy and interlaced state.

ii. The results of a one-factor experiment showed that the dosage of the GO/β-CD composite was positively correlated with the adsorption of methylene blue. The higher the dosage is, the greater the removal rate due to the excellent adsorption performance of the composite material, resulting in vacant adsorption sites in low-concentration solutions. With increasing temperature and contact time, the adsorption of methylene blue on GO/β-CD initially increased and then stabilized. Similarly, for the initial concentration of methylene blue, there was an initial increase followed by stabilization. For the initial concentration of methylene blue, the higher the concentration was, the lower the removal rate of the composite material. This is mainly because the adsorption capacity of the composite material is fixed. The adsorption of methylene blue by GO/β-CD in neutral and alkaline environments is effective, while its efficiency is slightly reduced in acidic environments.

iii. Through adsorption isotherm, adsorption kinetics, and adsorption thermodynamics models fitting, the following conclusions were drawn: the adsorption of MB by the GO/β-CD composite was attributed to the adsorption of the monomolecular layer, and the adsorption was dominated by chemical adsorption accompanied by physical adsorption. The epoxy carboxylation reaction of GO and β-CD branching produces carboxylated active sites and many functional groups, so that the composite material has a large adsorption capacity. The diffusion within the particles is dominated by macroporous diffusion, which is the main influence on the diffusion of MB in the particles. The intraparticle diffusion is primarily influenced by macroporous diffusion, which is a key factor affecting the adsorption rate.

Therefore, GO/β-CD composites have great potential as an adsorbent and play a crucial role in the adsorption treatment of dye wastewater. In the future, we will optimise the adsorbent materials, further

explore the adsorption mechanism, and investigate the application of the adsorbent in real water bodies. And we will expand the application field of GO/β-CD, which is widely used in the removal of pollutants from wastewater, environmental remediation and wastewater treatment facilities. However, the commercialization of GO/β-CD composites will face challenges related to cost and large-scale production. Future research should focus on optimizing the production process, improving material properties, and exploring emerging markets and applications to improve industrial scalability and applicability.

Acknowledgements The authors would like to express their gratitude to Research Program of Qilu Institute of Technology (No.: QIT23NK002) and the Ministry of Higher Education Malaysia for providing research funding through the Fundamental Research Grant Scheme (Grant Number: FRGS/1/2020/WAB02/UNIMAS/03/1). The authors also thank Qilu Institute of Technology and Universiti Malaysia Sarawak for their support in this work.

Funding Research Program of Qilu Institute of Technology, QIT23NK002,Yanping Qu, and the Ministry of Higher Education Malaysia forproviding research funding through the Fundamental Research Grant Scheme, FRGS/1/2020/WAB02/UNIMAS/03/1, Ibrahim Yakub

Data Availability The authors state that data supporting the results of this study are available in the paper and its supplementary information file. If the original data file is needed in other formats, it can be requested from the corresponding author. The original data is attached.

Declarations

Conflict of Interest The authors declare no conflicts of interest.

References

Abd El Salam, H. M. (2023). Bio-Sustainable Alternatives Synthesis of Nanoporous Activated Carbon @Al-MOF for the Adsorption of Hazardous Organic Dyes from Wastewater. *Water, Air, & Soil Pollution, 234*(9), 567. https://doi.org/10.1007/s11270-023-06572-6

Alsbaiee, A., Smith, B. J., Xiao, L., Ling, Y., Helbling, D. E., & Dichtel, W. R. (2016). Rapid removal of organic micropollutants from water by a porous β-cyclodextrin polymer. *Nature, 529*(7585), 190–194.

Alver, E., Metin, A. Ü., & Brouers, F. (2020). Methylene blue adsorption on magnetic alginate/rice husk bio-composite. *International Journal of Biological Macromolecules, 154*, 104–113.

Al-Yaari, M., & Saleh, T. A. (2023). Removal of Lead from Wastewater Using Synthesized Polyethyleneimine-Grafted Graphene Oxide. *Nanomaterials, 13*(6), 1078.

Bahadi, S. A., Drmosh, Q. A., & Onaizi, S. A. (2024). Adsorptive removal of organic pollutants from aqueous solutions using novel GO/bentonite/MgFeAl-LTH nanocomposite. *Environmental Research, 248*, 118218. https://doi.org/10.1016/j.envres.2024.118218

Borandeh, S., Hosseinbeigi, H., Abolmaali, S. S., Monajati, M., & Tamaddon, A. M. (2021). Steric stabilization of β-cyclodextrin functionalized graphene oxide by host-guest chemistry: A versatile supramolecule for dual-stimuli responsive cellular delivery of doxorubicin. *Journal of Drug Delivery Science and Technology, 63*, 102536.

Bucur, S., Diacon, A., Mangalagiu, I., Mocanu, A., Rizea, F., Dinescu, A., et al. (2021). Bisphenol A adsorption on silica particles modified with beta-cyclodextrins. *Nanomaterials, 12*(1), 39.

Chen, H., Zhou, Y., Wang, J., Lu, J., & Zhou, Y. (2020). Polydopamine modified cyclodextrin polymer as efficient adsorbent for removing cationic dyes and Cu2+. *Journal of Hazardous Materials, 389*, 121897.

Ching, C., Ling, Y., Trang, B., Klemes, M., Xiao, L., Yang, A., et al. (2022). Identifying the physicochemical properties of β-cyclodextrin polymers that determine the adsorption of perfluoroalkyl acids. *Water Research, 209*, 117938.

Chowdhury, I., Duch, M. C., Mansukhani, N. D., Hersam, M. C., & Bouchard, D. (2013). Colloidal Properties and Stability of Graphene Oxide Nanomaterials in the Aquatic Environment. *Environmental Science & Technology, 47*(12), 6288–6296. https://doi.org/10.1021/es400483k

Crini, G., & Morcellet, M. (2002). Synthesis and applications of adsorbents containing cyclodextrins. *Journal of Separation Science, 25*(13), 789–813. https://doi.org/10.1002/1615-9314(20020901)25:13%3c789::AID-JSSC789%3e3.0.CO;2-J

Dai, J., Zhao, C., Hu, X., Chen, D., Yun, J., Liu, C., et al. (2021). One-pot synthesis of meso-microporous ZSM-5 and its excellent performance in VOCs adsorption/desorption. *Journal of Chemical Technology & Biotechnology, 96*(1), 78–87. https://doi.org/10.1002/jctb.6510

De Figueiredo Neves, T., Kushima Assano, P., Rodrigues Sabino, L., Bardelin Nunes, W., & Prediger, P. (2020). Influence of Adsorbent/Adsorbate Interactions on the Removal of Cationic Surfactants from Water by Graphene Oxide. *Water, Air, & Soil Pollution, 231*(6), 304. https://doi.org/10.1007/s11270-020-04669-w

Demircan Ozelcaglayan, E., Honek, J. F., & Parker, W. J. (2024). Molecular level investigation of interactions between pharmaceuticals and β-cyclodextrin (β-CD) functionalized adsorption sites for removal of pharmaceutical contaminants from water. *Chemosphere, 347*, 140639. https://doi.org/10.1016/j.chemosphere.2023.140639

Din, M. I., Khalid, R., Najeeb, J., & Hussain, Z. (2021). Fundamentals and photocatalysis of methylene blue dye using various nanocatalytic assemblies-a critical review. *Journal of Cleaner Production, 298*, 126567.

Dong, K., Jiang, Y., Zhang, Y., Qin, Z., & Mo, L. (2023). Tannic acid-assisted fabrication of antibacterial sodium alginate-based gel beads for the multifunctional adsorption of

heavy metal ions and dyes. *International Journal of Biological Macromolecules, 252*, 126249.

Fan, Q., Zhang, L., Xing, H., Wang, H., & Ji, X. (2020). Microwave absorption and infrared stealth performance of reduced graphene oxide-wrapped Al flake. *Journal of Materials Science: Materials in Electronics, 31*(4), 3005–3016. https://doi.org/10.1007/s10854-019-02844-2

Ferrari, A. C. (2007). Raman spectroscopy of graphene and graphite: Disorder, electron–phonon coupling, doping and nonadiabatic effects. *Solid State Communications, 143*(1–2), 47–57.

Fu, L., Lai, G., & Yu, A. (2015). Preparation of β-cyclodextrin functionalized reduced graphene oxide: Application for electrochemical determination of paracetamol. *Rsc Advances, 5*(94), 76973–76978.

Fu, C., Dong, X., Wang, S., & Kong, F. (2019). Synthesis of nanocomposites using xylan and graphite oxide for remediation of cationic dyes in aqueous solutions. *International Journal of Biological Macromolecules, 137*, 886–894.

Gan, D., Dou, J., Huang, Q., Huang, H., Chen, J., Liu, M., et al. (2020). Carbon nanotubes-based polymer nanocomposites: Bio-mimic preparation and methylene blue adsorption. *Journal of Environmental Chemical Engineering, 8*(2), 103525.

Gunes, B., Jaquet, Y., Sánchez, L., Pumarino, R., McGlade, D., Quilty, B., et al. (2021). Activated graphene oxide-calcium alginate beads for adsorption of methylene blue and pharmaceuticals. *Materials, 14*(21), 6343.

Habila, M. A., ALOthman, Z. A., ALOthman, M. R., & Hassouna, M. S. E.-D. (2022). Benzothiophene adsorptive desulfurization onto TrihexYl (tetradecyl) phosphonium dicyanamide ionic-liquid-modified renewable carbon: Kinetic, equilibrium and UV spectroscopy investigations. Molecules, 28(1), 298.

Javed, I., Javed, T., & Khan, M. N. (2021). A characteristic study of Zea mays L.(sweet corn) cobs for synthetic dye degradation from aqueous media. *Water Science and Technology, 83*(1), 52–62.

Jawad, A. H., Abdulhameed, A. S., Wilson, L. D., Syed-Hassan, S. S. A., ALOthman, Z. A., & Khan, M. R. (2021). High surface area and mesoporous activated carbon from KOH-activated dragon fruit peels for methylene blue dye adsorption: Optimization and mechanism study. Chinese Journal of Chemical Engineering, 32, 281–290.

Jemli, S., Lütke, S. F., Chamtouri, F., Ben Amara, F., Bejar, S., Oliveira, M. L. S., et al. (2024). A novel cartoon crosslinked β-cyclodextrin (C-β-CD) polymer for effective uptake of Hg from aqueous solutions: Kinetics, equilibrium, thermodynamics, and statistical physics approach. *Separation and Purification Technology, 330*, 125578. https://doi.org/10.1016/j.seppur.2023.125578

Koçak, N., Çoktaş, F., Şimşek, S., Kaya, S., & Maslow, M. (2024). Preparation of Eco-Friendly Composite Material for Mercury (II) Adsorption Including Non-Wood Content From Walnut Green Husk (Juglon Regia L.): Experimental and Theoretical Studies. *Water, Air, & Soil Pollution, 235*(7), 453. https://doi.org/10.1007/s11270-024-07200-7

Li, Y., Yu, E., Sun, S., Liu, W., Hu, R., & Xu, L. (2022). Fast and highly efficient adsorption of cationic dyes by phytic acid crosslinked β-cyclodextrin. *Carbohydrate Polymers, 284*, 119231.

Lin, Y., Ma, J., Liu, W., Li, Z., & He, K. (2019). Efficient removal of dyes from dyeing wastewater by powder activated charcoal/titanate nanotube nanocomposites: Adsorption and photoregeneration. *Environmental Science and Pollution Research, 26*(10), 10263–10273. https://doi.org/10.1007/s11356-019-04218-x

Liu, H., Cai, X., Wang, Y., & Chen, J. (2011). Adsorption mechanism-based screening of cyclodextrin polymers for adsorption and separation of pesticides from water. *Water Research, 45*(11), 3499–3511.

Liu, X., Tian, J., Li, Y., Sun, N., Mi, S., Xie, Y., & Chen, Z. (2019). Enhanced dyes adsorption from wastewater via Fe3O4 nanoparticles functionalized activated carbon. *Journal of Hazardous Materials, 373*, 397–407.

Nayak, A., Sahoo, J. K., Sahoo, S. K., & Sahu, D. (2022). Removal of congo red dye from aqueous solution using zinc oxide nanoparticles synthesised from Ocimum sanctum (Tulsi leaf): A green approach. *International Journal of Environmental Analytical Chemistry, 102*(19), 7889–7910. https://doi.org/10.1080/03067319.2020.1842386

Nguyen, X. C., Nguyen, T. T. H., Nguyen, T. H. C., Van Le, Q., Vo, T. Y. B., Tran, T. C. P., et al. (2021). Sustainable carbonaceous biochar adsorbents derived from agro-wastes and invasive plants for cation dye adsorption from water. *Chemosphere, 282*, 131009.

Osagie, C., Othmani, A., Ghosh, S., Malloum, A., Esfahani, Z. K., & Ahmadi, S. (2021). Dyes adsorption from aqueous media through the nanotechnology: A review. *Journal of Materials Research and Technology, 14*, 2195–2218.

Ozelcaglayan, E. D., & Parker, W. J. (2023). β-Cyclodextrin functionalized adsorbents for removal of organic micropollutants from water. *Chemosphere, 320*, 137964.

Parimelazhagan, V., Yashwath, P., Arukkani Pushparajan, D., & Carpenter, J. (2022). Rapid removal of toxic Remazol brilliant blue-R dye from aqueous solutions using Juglans nigra shell biomass activated carbon as potential adsorbent: Optimization, isotherm, kinetic, and thermodynamic investigation. *International Journal of Molecular Sciences, 23*(20), 12484.

Qu, J., Dong, M., Wei, S., Meng, Q., Hu, L., Hu, Q., et al. (2020). Microwave-assisted one pot synthesis of β-cyclodextrin modified biochar for concurrent removal of Pb (II) and bisphenol a in water. *Carbohydrate Polymers, 250*, 117003.

Raees, A., Jamal, M. A., Ahmed, I., Silanpaa, M., & Saad Algarni, T. (2021). Synthesis and characterization of CeO2/CuO nanocomposites for photocatalytic degradation of methylene blue in visible light. *Coatings, 11*(3), 305.

Rajendran, S., Priya, T. A. K., Khoo, K. S., Hoang, T. K., Ng, H.-S., Munawaroh, H. S. H., et al. (2022). A critical review on various remediation approaches for heavy metal contaminants removal from contaminated soils. *Chemosphere, 287*, 132369.

Rápó, E., & Tonk, S. (2021). Factors affecting synthetic dye adsorption; desorption studies: A review of results from the last five years (2017–2021). *Molecules, 26*(17), 5419.

Rezakazemi, M., & Shirazian, S. (2019). Lignin-chitosan blend for methylene blue removal: Adsorption modeling. *Journal of Molecular Liquids, 274*, 778–791.

Sadiq, A. C., Olasupo, A., Ngah, W. S. W., Rahim, N. Y., & Suah, F. B. M. (2021). A decade development in the application of chitosan-based materials for dye adsorption: A short review. *International Journal of Biological Macromolecules, 191*, 1151–1163.

Samsami, S., Mohamadizaniani, M., Sarrafzadeh, M.-H., Rene, E. R., & Firoozbahr, M. (2020). Recent advances in the treatment of dye-containing wastewater from textile industries: Overview and perspectives. *Process Safety and Environmental Protection, 143*, 138–163.

Shi, Y., Wang, H., Song, G., Zhang, Y., Tong, L., Sun, Y., & Ding, G. (2022). Magnetic graphene oxide for methylene blue removal: Adsorption performance and comparison of regeneration methods. *Environmental Science and Pollution Research, 29*(20), 30774–30789. https://doi.org/10.1007/s11356-021-17654-5

Tene, T., Bellucci, S., Guevara, M., Arias Arias, F., Sáez Paguay, M. Á., Quispillo Moyota, J. M., et al. (2022). Adsorption of mercury on oxidized graphenes. *Nanomaterials, 12*(17), 3025.

Toan, T. Q., Ngan, T. K., Huong, D. T., Le, P.-A., Thuy, N. T., Huy, N. N., et al. (2023). Green and Facile Synthesis of Porous SiO_2 @C Adsorbents from Rice Husk: Preparation, Characterization, and Their Application in Removal of Reactive Red 120 in Aqueous Solution. *ACS Omega, 8*(11), 9904–9918. https://doi.org/10.1021/acsomega.2c07034

Usman, M., Ahmed, A., Yu, B., Wang, S., Shen, Y., & Cong, H. (2021). Simultaneous adsorption of heavy metals and organic dyes by β-Cyclodextrin-Chitosan based cross-linked adsorbent. *Carbohydrate Polymers, 255*, 117486.

Wang, J., Chen, Z., & Chen, B. (2014). Adsorption of Polycyclic Aromatic Hydrocarbons by Graphene and Graphene Oxide Nanosheets. *Environmental Science & Technology, 48*(9), 4817–4825. https://doi.org/10.1021/es405227u

Wang, J., Zhang, W., & Wei, J. (2019). Fabrication of poly (β-cyclodextrin)-conjugated magnetic graphene oxide by surface-initiated RAFT polymerization for synergetic adsorption of heavy metal ions and organic pollutants. *Journal of Materials Chemistry A, 7*(5), 2055–2065.

Wang, A., He, M., Ouyang, W., Lin, C., & Liu, X. (2021). Effects of antimony (III/V) on microbial activities and bacterial community structure in soil. *Science of the Total Environment, 789*, 148073.

Xu, W., Liu, X., & Tang, K. (2022). Adsorption of hydroquinone and Pb (II) from water by β-cyclodextrin/polyethyleneimine bi-functional polymer. *Carbohydrate Polymers, 294*, 119806.

Yağmur, H. K., & Kaya, İ. (2021). Synthesis and characterization of magnetic ZnCl2-activated carbon produced from coconut shell for the adsorption of methylene blue. *Journal of Molecular Structure, 1232*, 130071.

Yang, H., Shan, J., Li, J., & Jiang, S. (2019a). Microwave desorption and regeneration methods for activated carbon with adsorbed radon. *Adsorption, 25*(2), 173–185. https://doi.org/10.1007/s10450-019-00019-3

Yang, S., Wang, F., Tang, Q., Wang, P., Xu, Z., & Liang, J. (2019b). Utilization of ultra-light carbon foams for the purification of emulsified oil wastewater and their adsorption kinetics. *Chemical Physics, 516*, 139–146.

Yang, Z., Liu, X., Liu, X., Wu, J., Zhu, X., Bai, Z., & Yu, Z. (2021). Preparation of β-cyclodextrin/graphene oxide and its adsorption properties for methylene blue. *Colloids and Surfaces b: Biointerfaces, 200*, 111605.

Yilmaz, M. S. (2022). Graphene oxide/hollow mesoporous silica composite for selective adsorption of methylene blue. *Microporous and Mesoporous Materials, 330*, 111570.

Yu, F., Tian, F., Zou, H., Ye, Z., Peng, C., Huang, J., et al. (2021). ZnO/biochar nanocomposites via solvent free ball milling for enhanced adsorption and photocatalytic degradation of methylene blue. *Journal of Hazardous Materials, 415*, 125511.

Zainal, S. H., Mohd, N. H., Suhaili, N., Anuar, F. H., Lazim, A. M., & Othaman, R. (2021). Preparation of cellulose-based hydrogel: A review. *Journal of Materials Research and Technology, 10*, 935–952.

Zakaria, A. F., Kamaruzaman, S., Abdul Rahman, N., & Yahaya, N. (2022). Sodium Alginate/β-Cyclodextrin Reinforced Carbon Nanotubes Hydrogel as Alternative Adsorbent for Nickel (II) Metal Ion Removal. *Polymers, 14*(24), 5524.

Zghal, S., Jedidi, I., Cretin, M., Cerneaux, S., & Abdelmouleh, M. (2023). Adsorptive removal of Rhodamine B dye using carbon graphite/cnt composites as adsorbents: Kinetics, isotherms and thermodynamic study. *Materials, 16*(3), 1015.

Zhao, X., Wang, X., & Lou, T. (2021). Preparation of fibrous chitosan/sodium alginate composite foams for the adsorption of cationic and anionic dyes. *Journal of Hazardous Materials, 403*, 124054.

Zhu, L., Zhu, P., You, L., & Li, S. (2019). Bamboo shoot skin: Turning waste to a valuable adsorbent for the removal of cationic dye from aqueous solution. *Clean Technologies and Environmental Policy, 21*(1), 81–92. https://doi.org/10.1007/s10098-018-1617-0

Zhu, G., Xiao, Z., Yu, G., Zhu, G., Niu, Y., & Liu, J. (2021). Formation and characterization of furfuryl mercaptan-β-cyclodextrin inclusion complex and its thermal release characteristics. *Polish Journal of Chemical Technology, 23*(4), 35–40. https://doi.org/10.2478/pjct-2021-0035

Terms and Conditions

Springer Nature journal content, brought to you courtesy of Springer Nature Customer Service Center GmbH (“Springer Nature”).
Springer Nature supports a reasonable amount of sharing of research papers by authors, subscribers and authorised users (“Users”), for small-scale personal, non-commercial use provided that all copyright, trade and service marks and other proprietary notices are maintained. By accessing, sharing, receiving or otherwise using the Springer Nature journal content you agree to these terms of use (“Terms”). For these purposes, Springer Nature considers academic use (by researchers and students) to be non-commercial.
These Terms are supplementary and will apply in addition to any applicable website terms and conditions, a relevant site licence or a personal subscription. These Terms will prevail over any conflict or ambiguity with regards to the relevant terms, a site licence or a personal subscription (to the extent of the conflict or ambiguity only). For Creative Commons-licensed articles, the terms of the Creative Commons license used will apply.
We collect and use personal data to provide access to the Springer Nature journal content. We may also use these personal data internally within ResearchGate and Springer Nature and as agreed share it, in an anonymised way, for purposes of tracking, analysis and reporting. We will not otherwise disclose your personal data outside the ResearchGate or the Springer Nature group of companies unless we have your permission as detailed in the Privacy Policy.
While Users may use the Springer Nature journal content for small scale, personal non-commercial use, it is important to note that Users may not:

1. use such content for the purpose of providing other users with access on a regular or large scale basis or as a means to circumvent access control;
2. use such content where to do so would be considered a criminal or statutory offence in any jurisdiction, or gives rise to civil liability, or is otherwise unlawful;
3. falsely or misleadingly imply or suggest endorsement, approval , sponsorship, or association unless explicitly agreed to by Springer Nature in writing;
4. use bots or other automated methods to access the content or redirect messages
5. override any security feature or exclusionary protocol; or
6. share the content in order to create substitute for Springer Nature products or services or a systematic database of Springer Nature journal content.

In line with the restriction against commercial use, Springer Nature does not permit the creation of a product or service that creates revenue, royalties, rent or income from our content or its inclusion as part of a paid for service or for other commercial gain. Springer Nature journal content cannot be used for inter-library loans and librarians may not upload Springer Nature journal content on a large scale into their, or any other, institutional repository.
These terms of use are reviewed regularly and may be amended at any time. Springer Nature is not obligated to publish any information or content on this website and may remove it or features or functionality at our sole discretion, at any time with or without notice. Springer Nature may revoke this licence to you at any time and remove access to any copies of the Springer Nature journal content which have been saved.
To the fullest extent permitted by law, Springer Nature makes no warranties, representations or guarantees to Users, either express or implied with respect to the Springer nature journal content and all parties disclaim and waive any implied warranties or warranties imposed by law, including merchantability or fitness for any particular purpose.
Please note that these rights do not automatically extend to content, data or other material published by Springer Nature that may be licensed from third parties.
If you would like to use or distribute our Springer Nature journal content to a wider audience or on a regular basis or in any other manner not expressly permitted by these Terms, please contact Springer Nature at

onlineservice@springernature.com